



Article

Coordination-Driven Rare Earth Fractionation in Kuliokite-(Y), (Y,HREE)₄Al(SiO₄)₂(OH)₂F₅: A Crystal–Chemical Study

Sergey V. Krivovichev ^{1,2,*} , Victor N. Yakovenchuk ^{1,3}, Olga F. Goychuk ¹  and Yakov A. Pakhomovsky ^{1,3}

¹ Nanomaterials Research Center, Kola Science Center, Russian Academy of Sciences, Fersmana Str. 14, 184209 Apatity, Russia; v.yakovenchuk@ksc.ru (V.N.Y.); o.goychuk@ksc.ru (O.F.G.); y.pakhomovskiy@ksc.ru (Y.A.P.)

² Department of Crystallography, Institute of Earth Sciences, St. Petersburg State University, University Emb. 7/9, 199034 St. Petersburg, Russia

³ Geological Institute, Kola Science Center, Russian Academy of Sciences, Fersmana Str. 14, 184209 Apatity, Russia

* Correspondence: skrivovi@mail.ru

Abstract

The crystal structure of kuliokite-(Y), Y₄Al(SiO₄)₂(OH)₂F₅, has been re-investigated using the material from the type locality the Ploskaya Mt, Kola peninsula, Russian Arctic. It has been shown that in contrast to previous studies, the mineral is monoclinic, *Im*, with *a* = 4.3213(1), *b* = 14.8123(6), *c* = 8.6857(3) Å, β = 102.872(4)°, and *V* = 541.99(3) Å³. The crystal structure was solved and refined to *R*₁ = 0.030 on the basis of 3202 unique observed reflections. The average chemical composition determined by electron microprobe analysis is (Y_{2.96}Yb_{0.49}Er_{0.27}Dy_{0.13}Tm_{0.07}Lu_{0.05}Ho_{0.05}Gd_{0.01}Ca_{0.01})_{Σ4.04}Al_{0.92}Si_{2.04}O₈[(OH)_{2.61}F_{4.42}]_{Σ7.03}; the idealized formula is (Y,Yb,Er)₄Al[SiO₄]₂(OH)_{2.5}F_{4.5}. The crystal structure of kuliokite-(Y) contains two symmetrically independent Y sites, Y1 and Y2, coordinated by eight and seven X anions, respectively (X = O, F). The coordination polyhedra can be described as a distorted square antiprism and a distorted pentagonal bipyramid, respectively. The refinement of site occupancies indicated that the mineral represents a rare case of HREE fractionation among two cation sites driven by their coordination numbers and geometry. In agreement with the lanthanide contraction, HREEs are selectively incorporated into the Y2 site with a smaller coordination number and tighter coordination environment. The strongest building unit of the structure is the [AlX₂(SiO₄)₂] chain of corner-sharing AlX₆ octahedra and SiO₄ tetrahedra running along the *a* axis. The chains have their planes oriented parallel to (001). The Y atoms are located in between the chains, along with the F[−] and (OH)[−] anions, providing the three-dimensional integrity of the crystal structure. Each F[−] anion is coordinated by three Y³⁺ cations to form planar (FY₃)⁸⁺ triangles parallel to the (010) plane. The triangles share common edges to form [F₂Y₂]⁴⁺ chains parallel to the *a* axis. The analysis of second-neighbor coordination of Y sites allowed us to identify the structural topology of kuliokite-(Y) as the only case of the *skd* network in inorganic compounds, previously known in molecular structures only. The variety of anionic content in the mineral allows us to identify the potential existence of two other mineral species that can tentatively be named ‘fluorokuliokite-(Y)’ and ‘hydroxykuliokite-(Y)’.

Keywords: rare earth minerals; crystal structure; lanthanoid contraction; coordination chemistry; kuliokite-(Y); rare earth fractionation; Russian Arctic



Received: 27 August 2025

Revised: 1 October 2025

Accepted: 9 October 2025

Published: 10 October 2025

Citation: Krivovichev, S.V.; Yakovenchuk, V.N.; Goychuk, O.F.; Pakhomovsky, Y.A. Coordination-Driven Rare Earth Fractionation in Kuliokite-(Y), (Y,HREE)₄Al(SiO₄)₂(OH)₂F₅: A Crystal–Chemical Study. *Minerals* **2025**, *15*, 1064. <https://doi.org/10.3390/min15101064>

Copyright: © 2025 by the authors. Licensee MDPI, Basel, Switzerland. This article is an open access article distributed under the terms and conditions of the Creative Commons Attribution (CC BY) license (<https://creativecommons.org/licenses/by/4.0/>).

1. Introduction

Natural minerals are the key source of rare earth elements (REEs) due to their industrial and technological use, and REE mineral resources have received enormous attention from both geological and economic points of view [1–5]. Rare earth minerals are very diverse chemically as well as structurally, and a large number of new mineral species have been discovered over recent years [6–29]. Of particular interest are minerals that contain heavy REEs (HREEs) such as Yb, owing to their importance in the fabrication of materials for lasers, superconductors, atomic clocks, ion qubits, etc. There are four mineral species that contain Yb as a mineral-forming component (i.e., when Yb dominates over other elements at least in one structural site): xenotime-(Yb), YbPO_4 [30], samarskite-(Yb), YbNbO_4 [31], hingganite-(Yb), $\text{YbBe}(\text{SiO}_4)(\text{OH})$ [32], and keiviite-(Yb), $\text{Yb}_2\text{Si}_2\text{O}_7$ [33]. The origin of the four Yb minerals is connected with granitic pegmatites, where Yb concentrates in Y minerals *sensu stricto*. The most important geographic localities where Yb minerals have been found are: Ploskaya Mountain (Mt) pegmatites (Kola peninsula, Russia), Stetind and Høydalen pegmatites (Norway), Shatford Lake pegmatites (Manitoba, Canada), Little Patsy pegmatites (Colorado, U.S.), Zudong granites (Jiangxi, China), etc. Among them, amazonitic pegmatites of the Ploskaya Mt are unique as a type locality for two Yb minerals, hingganite-(Yb) and keiviite-(Yb), where xenotime-(Yb) was found as well [34]. In addition, the Ploskaya Mt is the type locality for kuliokite-(Y) that contains essential amounts of Yb and is the subject of this study.

Kuliokite-(Y) was discovered by Voloshin et al. [35] in amazonitic pegmatites of the Kola peninsula (Russia) in close association with thalenite-(Y) and keiviite-(Y). Later, it was also found in two localities in Norway: Høydalen (southern Norway) [36] and Stetind (northern Norway) [37]. The mineral was named after the Kuliok river located in the central part of the Kola peninsula. It is of interest that the mineral has no synthetic analogues and had never been prepared under laboratory conditions. The crystal structure of kuliokite-(Y) was reported by Sokolova et al. [38] to be triclinic and non-centrosymmetric, with the space group $P1$, $a = 8.606$, $b = 8.672$, $c = 4.317$ Å, $\alpha = 102.79$, $\beta = 97.94$, $\gamma = 116.66^\circ$, and $V = 270.1$ Å³. The empirical chemical formula of the mineral was reported as $(\text{Y}_{3.58}\text{Yb}_{0.10}\text{Er}_{0.085}\text{Dy}_{0.055}\text{Gd}_{0.015}\text{Lu}_{0.005}\text{Ho}_{0.005})\text{Al}_{1.04}\text{Si}_{2.12}\text{O}_{7.59}\text{F}_{5.08}(\text{OH})_{2.88}$; the ideal formula is $\text{Y}_4\text{Al}(\text{SiO}_4)_2(\text{OH})_2\text{F}_5$. Our re-investigation of the natural material from the type locality demonstrated that kuliokite-(Y) is, in fact, monoclinic and contains two REE sites that are selective with respect to the HREEs. Site selectivity is controlled by the coordination features (coordination number and geometry), in agreement with the lanthanoid contraction.

2. Materials and Methods

2.1. Materials

The crystals of kuliokite-(Y) used in this study have been found in amazonitic pegmatites of the Ploskaya Mt, Keivy massif, Kola peninsula, Russian Arctic. Kuliokite-(Y) forms pinkish transparent crystals (Figure 1) in association with albite, aegirine, thalénite, xenotime-(Y), and kainosite-(Y).



Figure 1. Pinkish crystals of kuliokite-(Y) in association with albite (white), amazonite (green), and aegirine (black) from the Ploskaya Mt, Kola peninsula, Russian Arctic. The field of view is ca. $2 \times 3 \text{ mm}^2$.

2.2. Chemical Composition

The chemical composition of kuliokite-(Y) has been studied by wavelength dispersion spectrometry using a Cameca MS-46 electron microprobe (Geological Institute, Kola Science Centre of the Russian Academy of Sciences, Apatity, Russia) operating at 20 kV, 20–30 nA, and with a $5 \mu\text{m}$ beam diameter. Table 1 provides the mean analytical results for three kuliokite crystals (where each analysis is the average of 4–7 point measurements). The standards used for the microprobe work are as follows: synthetic $\text{Y}_3\text{Al}_5\text{O}_{12}$ (Y and Al), synthetic $\text{LiREE}(\text{MoO}_4)_2$ (REE = Yb, Er, Lu, Tm, Gd), $\text{LiREE}'(\text{WO}_4)_2$ (REE' = Dy and Ho), diopside (Ca and Si), and fluorite (F).

Table 1. Chemical composition of kuliokite-(Y) (in wt.% and atoms per formula unit (apfu)), and mean site-scattering factors ($\langle\text{SSF}\rangle$, e^-) for the Y site in its crystal structure.

Oxide	1	2	3	Average	Atom	1	2	3	Average
Al_2O_3	5.76	5.94	6.11	5.94	Al	0.91	0.92	0.93	0.92
SiO_2	15.36	15.55	15.68	15.53	Si	2.05	2.04	2.03	2.04
CaO	–	0.14	0.07	0.07	Ca	–	0.02	0.01	0.01
Y_2O_3	40.32	41.68	45.10	42.37	Y	2.86	2.91	3.11	2.96
Gd_2O_3	0.27	0.34	0.28	0.30	Gd	0.01	0.01	0.01	0.01
Dy_2O_3	2.69	2.90	3.34	2.98	Dy	0.12	0.12	0.14	0.13
Ho_2O_3	0.98	1.17	1.11	1.09	Ho	0.04	0.05	0.05	0.05
Er_2O_3	6.69	6.59	6.35	6.54	Er	0.28	0.27	0.26	0.27
Tm_2O_3	1.87	1.71	1.41	1.66	Tm	0.08	0.07	0.06	0.07
Yb_2O_3	14.46	13.04	9.48	12.33	Yb	0.59	0.52	0.37	0.49
Lu_2O_3	1.61	1.47	0.76	1.28	Lu	0.06	0.06	0.03	0.05
F	10.45	10.45	10.99	10.63	F	4.41	4.34	4.50	4.42
	100.46	100.98	100.68	100.71	OH	2.64	2.68	2.52	2.61
$-\text{O}=\text{F}_2$	−4.40	−4.40	−4.63	−4.48	$\langle\text{SSF}\rangle$, e^-	48.23	47.41	46.14	47.31
$\text{H}_2\text{O}_{\text{calc}}$ *	2.97	3.07	2.92	2.99					
Total	99.03	99.65	98.97	99.22					

* calculated from crystal structure data.

The average empirical chemical formula calculated on the basis of $\text{Al} + \text{Si} + \text{Ca} + \text{Y} + \text{Gd} + \text{Dy} + \text{Ho} + \text{Er} + \text{Tm} + \text{Yb} + \text{Lu} = 7$ can be written as $(\text{Y}_{2.96}\text{Yb}_{0.49}\text{Er}_{0.27}\text{Dy}_{0.13}\text{Tm}_{0.07}\text{Lu}_{0.05}\text{Ho}_{0.05}\text{Gd}_{0.01}\text{Ca}_{0.01})_{\Sigma 4.04}\text{Al}_{0.92}\text{Si}_{2.04}\text{O}_8[(\text{OH})_{2.61}\text{F}_{4.42}]_{\Sigma 7.03}$; the idealized formula is $(\text{Y,Yb,Er})_4\text{Al}[\text{SiO}_4]_2(\text{OH})_{2.5}\text{F}_{4.5}$, which is close to that reported earlier, $\text{Y}_4\text{Al}(\text{SiO}_4)_2(\text{OH})_2\text{F}_5$ [35]. It is notable that our kuliokite-(Y) sample contains less F, but more Yb and Er, than the crystals of the mineral used in the original study by Voloshin et al. [35]. The differences in chemical composition between the samples will be discussed below.

2.3. Single-Crystal X-Ray Diffraction Analysis

The crystal structure study of kuliokite-(Y) was carried out by means of the Synergy S single-crystal diffractometer equipped with the Hypix detector using monochromatic $\text{MoK}\alpha$ radiation ($\lambda = 0.71069 \text{ \AA}$) at room temperature. More than a half of the diffraction sphere was collected using a scanning step of 1° and an exposure time of 60 s. The data were integrated and corrected by means of the CrysAlis 1.171.36.20 program package, which was also used to apply empirical absorption correction using spherical harmonics, implemented in the SCALE3 ABSPACK scaling algorithm [39]. The structure was solved and refined using the SHELXL2015 software package [40].

The crystal structure of kuliokite-(Y) was solved by using direct methods in the monoclinic non-centrosymmetric space group Im , in contrast to the original study by Sokolova et al. [38], who reported the structure in the triclinic space group $P1$. The unit cell vectors ($\mathbf{a}_t, \mathbf{b}_t, \mathbf{c}_t$) determined in this work (Table 2) are related to those determined in [38] ($\mathbf{a}_s, \mathbf{b}_s, \mathbf{c}_s$) through the following equations:

$$\mathbf{a}_t = -\mathbf{c}_s; \mathbf{b}_t = 2\mathbf{a}_s + \mathbf{b}_s + \mathbf{c}_s; \mathbf{c}_t = -\mathbf{b}_s \quad (1)$$

Table 2. Crystal data and structure refinement for kuliokite-(Y).

Temperature (K)	293(2)
Crystal system	monoclinic
Space group	Im
a (Å)	4.32130(10)
b (Å)	14.8123(6)
c (Å)	8.6857(3)
β ($^\circ$)	102.872(4)
Volume (Å ³)	541.99(3)
Z	2
ρ_{calc} (g/cm ³)	4.723
μ (mm ^{−1})	24.620
$F(000)$	702
Crystal size (mm ³)	$0.17 \times 0.12 \times 0.10$
Radiation	$\text{MoK}\alpha$ ($\lambda = 0.71073$)
2Θ range for data collection/ $^\circ$	9.56–82.14
Index ranges	$-7 \leq h \leq 7, -27 \leq k \leq 26, -15 \leq l \leq 15$
Reflections collected	8540
Independent reflections	3202 [$R_{\text{int}} = 0.0301, R_{\text{sigma}} = 0.0428$]
Data/restraints/parameters	3202/3/117
Flack parameter	0.969(12)
Goodness-of-fit (S) on F^2	1.153
Weighting scheme	$W = 1/[S^2(F_o^2) + (0.0578P)^2 + 1.6209P]$, where $P = (F_o^2 + 2F_c^2)/3$

Table 2. Cont.

Final R indexes [$I \geq 4\sigma(I)$]	$R_1 = 0.030$, $wR_2 = 0.087$
Final R indexes [all data]	$R_1 = 0.030$, $wR_2 = 0.087$
Largest diff. peak/hole/ $e \text{ \AA}^{-3}$	3.434/−2.366

The respective transformation matrix is $[00\bar{1}/211/\bar{1}00]$. The reciprocal transformation matrix $[(a_t, b_t, c_t) \rightarrow (a_s, b_s, c_s)]$ is $[\frac{1}{2}\frac{1}{2}\frac{1}{2}/00\bar{1}/\bar{1}00]$. The unit cell parameters for the primitive cell similar to that reported in [38] are $a_s = 8.614$, $b_s = 8.686$, $c_s = 4.321 \text{ \AA}$, $\alpha_s = 102.87^\circ$, $\beta_s = 97.96^\circ$, $\gamma_s = 116.63^\circ$, which are almost the same as those given in the original work [38] (see above). The relations between the monoclinic and triclinic cells are shown in Figure 2. The monoclinic symmetry of kulikoite-(Y) revealed in our study is in agreement with the general observations of crystals of the mineral. For instance, Raade et al. [36] reported the pseudomonoclinic habit of kulikoite-(Y) crystals from the Høydaalen pegmatites. The structure model in the space group Im was checked for missing symmetry elements using PLATON 2023.1 software [41]; no additional symmetry was found. The racemic twin model was used in the final refinement; the obtained Flack parameter [42] is 0.969(12).

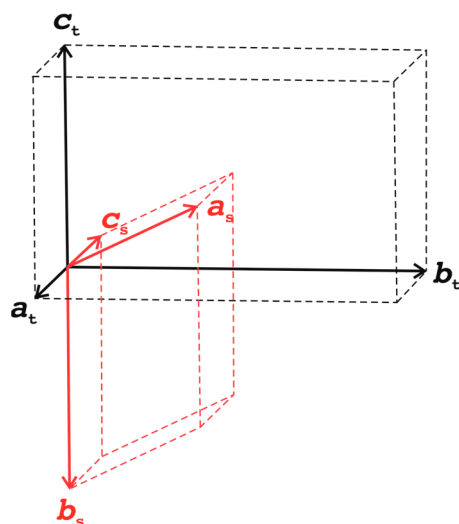


Figure 2. The relations between the unit cell vectors of kulikoite-(Y) determined in this work (in black) with those determined previously (red).

The position of one H site was located through the inspection of the difference Fourier maps of electron density; other H sites could not be located. The occupancies of the Y sites were refined using mixed Y-Yb scattering curves for neutral atoms; the procedure implemented in SHELXL [40] was applied with the Y and Yb curves used for the same site (two sites with the same coordinates and displacement parameters) and the total occupancy constrained to 1.0. Crystal data, data collection information, and structure refinement details are given in Table 2; atom coordinates and displacement parameters are given in Table 3, and selected interatomic distances are shown in Table 4. Table 5 provides the results of the bond valence analysis; the bond valence parameters for the cation–oxygen and cation–fluorine bonds have been taken from [43,44], respectively.

Table 3. Atomic coordinates, site occupancies, and displacement parameters (\AA^2) for kuliokite-(Y).

Site	Occupancy	x	y	z	U_{iso}
Y1	Y _{0.84} Yb _{0.16}	0.46546(8)	0.36988(3)	0.72252(5)	0.0053(1)
Y2	Y _{0.69} Yb _{0.31}	0.28434(5)	0.14586(2)	0.85270(4)	0.0053(1)
Si	Si	0.6186(4)	0.1555(1)	0.5428(2)	0.0045(3)
Al	Al	0.1137(6)	0	0.5499(3)	0.0056(4)
O1	O	0.7421(10)	0.2101(3)	0.4058(5)	0.0089(6)
O2	O	0.4979(10)	0.2189(3)	0.6712(5)	0.0086(6)
O3	O	0.3275(9)	0.0900(3)	0.4551(5)	0.0063(6)
O4	O	0.9081(10)	0.0925(3)	0.6426(5)	0.0072(6)
F1	F	0.4270(10)	0.1329(3)	0.1207(6)	0.0120(7)
F2	F	−0.171(1)	0.1398(3)	0.9452(6)	0.0111(7)
F3	F _{0.5} (OH) _{0.5} *	0.4082(14)	0	0.7581(7)	0.0102(8)
O5	OH	0.3136(14)	½	0.8570(8)	0.0092(8)
O6	OH	0.538(2)	½	0.6077(10)	0.019(1)
H	H	0.72(5)	½	0.56(4)	0.080 *

Site	U_{11}	U_{22}	U_{33}	U_{23}	U_{12}	U_{13}
Y1	0.0057(2)	0.0056(2)	0.0048(2)	−0.0009(1)	0.0018(1)	−0.0003(1)
Y2	0.0055(1)	0.0057(1)	0.0049(1)	−0.0008(1)	0.00181(9)	−0.0004(1)
Si	0.0050(5)	0.0048(6)	0.0042(5)	0.0000(5)	0.0020(4)	0.0002(4)
Al	0.0062(8)	0.0049(9)	0.0057(9)	0	0.0015(6)	0
O1	0.0127(14)	0.0072(14)	0.0082(14)	0.0035(11)	0.006(1)	0.001(12)
O2	0.0139(15)	0.0056(13)	0.0075(14)	−0.0003(11)	0.005(1)	−0.000(1)
O3	0.0046(12)	0.0084(14)	0.0060(13)	0.0002(10)	0.001(1)	−0.001(1)
O4	0.0063(12)	0.0083(14)	0.0061(14)	−0.0001(10)	−0.000(1)	0.001(1)
F1	0.0078(15)	0.0200(19)	0.0084(17)	0.0014(12)	0.002(1)	0.001(1)
F2	0.0061(14)	0.0193(18)	0.0085(18)	0.0004(11)	0.003(1)	−0.000(1)
F3	0.0102(19)	0.009(2)	0.010(2)	0	−0.001(2)	0
O5	0.010(2)	0.0081(19)	0.009(2)	0	0.0003(16)	0
O6	0.039(4)	0.007(2)	0.017(3)	0	0.019(3)	0

* fixed during refinement.

Table 4. Selected interatomic distances (\AA) for the crystal structure of kuliokite-(Y).

Y1–O6	2.225(4)	Y2–O1	2.199(4)
Y1–O2	2.291(4)	Y2–O2	2.270(4)
Y1–F1	2.298(5)	Y2–F1	2.280(5)
Y1–O3	2.340(4)	Y2–F2	2.288(4)
Y1–F2	2.353(5)	Y2–O4	2.297(4)
Y1–F1	2.355(5)	Y2–F2	2.312(4)
Y1–O1	2.357(4)	Y2–F3	2.413(3)
Y1–O5	2.419(4)	<Y2–X *>	2.294
<Y1–X *>	2.330		
		Si–O1	1.624(4)
Al–O5	1.877(7)	Si–O2	1.629(4)
Al–O4	1.906(4) 2×	Si–O3	1.637(4)
Al–O3	1.910(5) 2×	Si–O4	1.644(4)
Al–F3	1.966(6)	<Si–O>	1.634
<Al–X *>	1.913		

* X = O, F.

Table 5. Bond valence analysis (in valence units = v.u.) for kuliokite-(Y).

Atom	O1	O2	O3	O4	F1	F2	F3	O5	O6	Σ
Y1	0.39	0.46	0.41		0.34, 0.30	0.30		0.34 $^{2\times\downarrow}$	0.55 $^{2\times\downarrow}$	3.09
Y2	0.58	0.49		0.46	0.36	0.33, 0.35	0.25 $^{2\times\downarrow}$			2.82
Al			0.50 $^{2\times\rightarrow}$	0.50 $^{2\times\rightarrow}$			0.43	0.54		2.97
Si	1.00	0.99	0.97	0.95						3.91
Σ	1.97	1.94	1.88	1.91	1.00	0.98	0.93	1.22	1.10	

3. Results

3.1. Cation Coordination and Site Assignment

The crystal structure of kuliokite-(Y) contains two symmetrically independent Y sites, Y1 and Y2, coordinated by eight and seven X anions, respectively ($X = O, F$) (Figure 3). The coordination polyhedron of the Y1 site can be described as a distorted square antiprism formed by five O and three F atoms, whereas the Y2X₇ polyhedron is a distorted pentagonal bipyramid with $7X = 4O + 3F$. Both types of coordination are typical for inorganic rare earth compounds [45]. The average $\langle Y-X \rangle$ bond lengths are 2.330 and 2.294 Å for the Y1 and Y2 sites, respectively, which means that the Y2 coordination is more tight and is more suitable for smaller cations. This is in agreement with the observed site-scattering factor (SSF) values for the Y1 and Y2 sites equal to 43.96 and 48.61 e^- , respectively. According to this observation, in kuliokite-(Y), HREEs show selective preference for the smaller Y2 site, which agrees with the lanthanoid contraction, i.e., the gradual decrease in the atomic and ionic sizes of lanthanides from La to Lu [46,47]. Figure 4 shows the changes in ionic radii for the 7- and 8-coordinated REE³⁺ ions in comparison with Y³⁺ (based on the recent tabulation of ionic radii by Gagne and Hawthorne [48]). The ionic radii for the 7- and 8-coordinated Yb³⁺ cations are 0.959 and 0.991 Å, respectively, which are smaller than the respective radii for the Y³⁺ cations (0.966 and 1.024 Å, respectively). Thus, the observed fractionation of HREEs in the crystal structure of kuliokite-(Y) is governed by the coordination features (coordination number and geometry) of the Y sites.

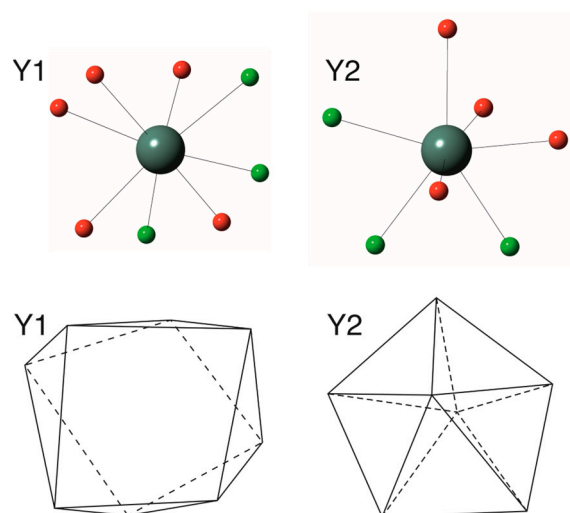


Figure 3. The coordination polyhedra of Y atoms in the crystal structure of kuliokite-(Y). Legend: Y, O, and F atoms are shown as gray, red, and green spheres, respectively.

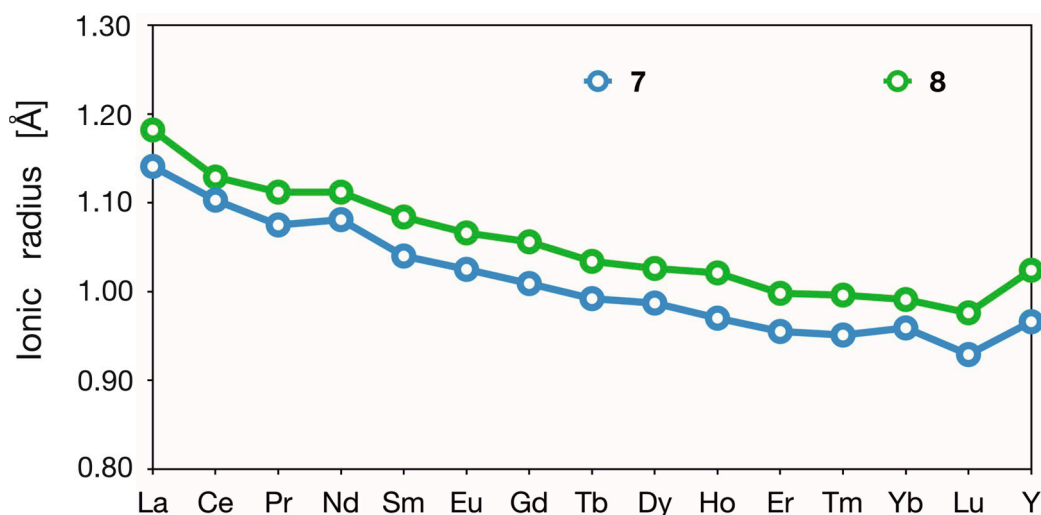


Figure 4. The ionic radii of trivalent lanthanide ions in [7]- and [8]-coordinated cations (blue and green, respectively) in comparison to Y^{3+} (on the right side of the diagram). The values of the ionic radii are taken from [48].

The average $\langle SSF \rangle$ value for the Y sites derived from crystal structure analysis is $46.29 e^-$, which is somewhat smaller than the average value of $47.31 e^-$ obtained from chemical analysis. However, it agrees well with the value of $46.14 e^-$ observed in the analysis 3 in Table 1. The variability in the HREE content in kuliokite-(Y) was mentioned in the original study [35], though our sample has a much higher HREE content than the holotype crystals.

3.2. Structure Description

The crystal structure of kuliokite-(Y) is shown in Figure 5a,b. The strongest building unit of the structure is the $[AlX_2(SiO_4)_2]$ chain of corner-sharing AlX_6 octahedra and SiO_4 tetrahedra running along the a axis (Figure 5c). The chains have their planes oriented parallel to (001). The Y atoms are located in between the chains, along with the F^- and $(OH)^-$ anions, providing the three-dimensional integrity of the crystal structure. Each F^- anion is coordinated by three Y^{3+} cations to form planar $(FY_3)^{8+}$ triangles parallel to the (010) plane. The triangles share common edges to form $[F_2Y_2]^{4+}$ chains, as shown in Figure 5d. The similar but isolated $(FY_3)^{8+}$ groups have also been observed in thalénite, $Y_3[Si_3O_{10}]F$ [49,50], and cappelenite-(Y), $BaY_6B_6Si_3O_{24}F_2$ [51].

Due to the relatively high coordination number of Y atoms and their varied coordination, providing a description of the crystal structure in terms of Y coordination polyhedra is difficult and non-transparent. An alternative description of the structural topology of kuliokite-(Y) may be devised using nodal representation [52,53], where each coordination polyhedron is designated by a node and two nodes are linked together by an edge, if the respective Y polyhedra share common ligands. In the crystal structure of kuliokite-(Y), each Y polyhedron is linked to six adjacent polyhedra by sharing common edges and corners (Figure 6). The $Y \cdots Y$ distances from central to adjacent Y sites do not exceed 4.5 \AA .

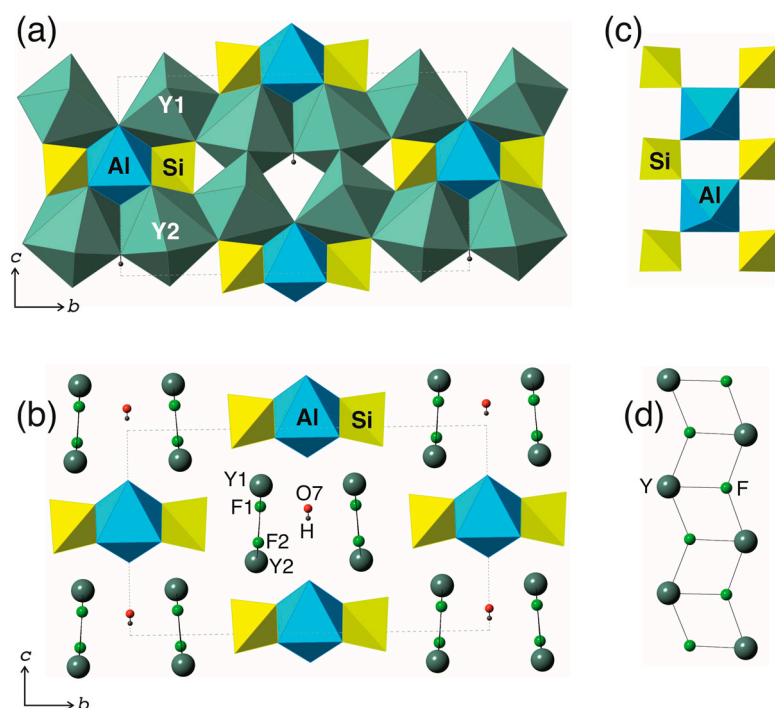


Figure 5. The crystal structure of kuliokite-(Y) projected along the a axis shown in polyhedral (a) and combined polyhedral and ball-and-stick (b) representations; the $[\text{AlX}_2(\text{SiO}_4)_2]$ chain (c) and the $[\text{F}_2\text{Y}_2]$ chain of (FY_3) triangular groups (d). Legend: Y, O, H, and F atoms are shown as gray, red, black, and green spheres, respectively; Y, Al, and Si coordination polyhedra are shown in greenish-gray, light-blue, and yellow colors, respectively.

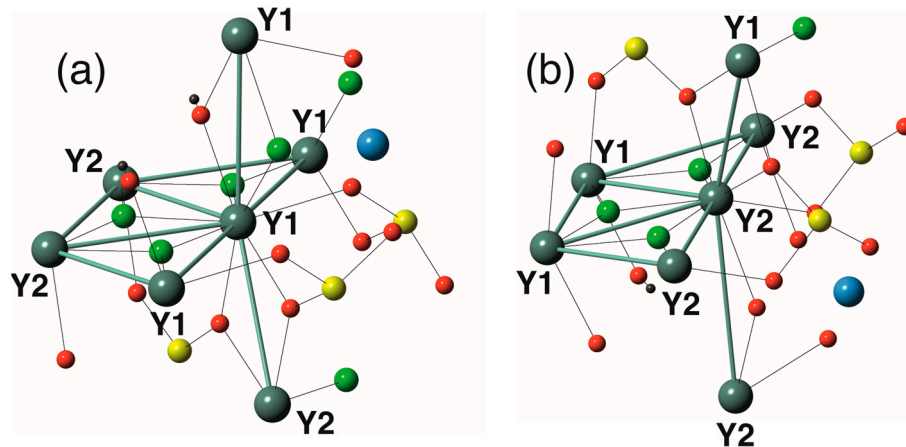


Figure 6. The atomic environment of the Y1 (a) and Y2 (b) sites in the crystal structure of kuliokite-(Y) within the 4.5 Å sphere. Legends as in Figures 3 and 5. The adjacent Y sites are linked by an edge if their coordination polyhedra share common O or F atoms.

If the Y sites located from each other within 4.5 Å are linked by edges, a three-dimensional Y network is obtained, which is shown in Figure 7a. The network contains 6-coordinated nodes and possesses channels that are parallel to the a axis and accommodate the one-dimensional blue-and-yellow graphs that reflect the topologies of linkage of AlX_6 and SiO_4 polyhedra of the aluminosilicate chains shown in Figure 5c.

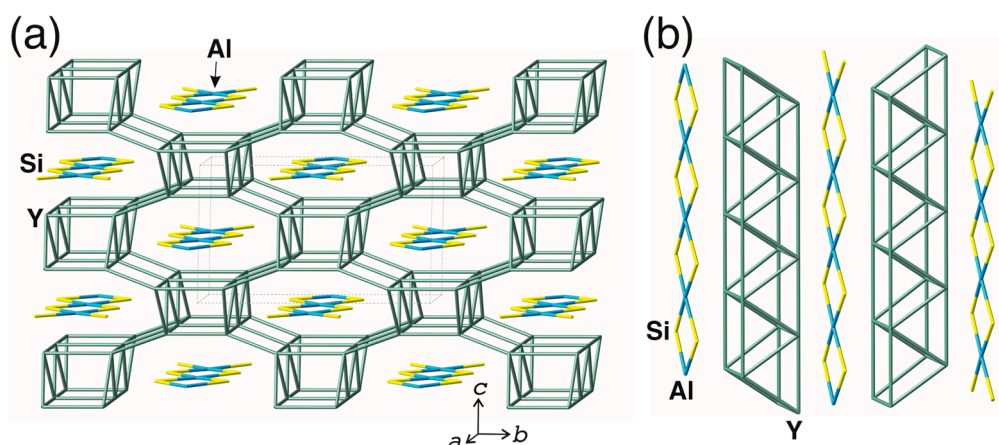


Figure 7. The crystal structure of kuliokite-(Y) shown as the Y network of the **skd** topology with channels occupied by Al-Si graphs corresponding to the aluminosilicate octahedral–tetrahedral chains (a); the spatial relations between the Al-Si chains and double Y chains (b).

It is remarkable that the topology of the Y network in kuliokite-(Y) is known in coordination chemistry and corresponds to the **skd** topology stored in the Reticular Chemistry Structure Resource (RCSR) [54,55]. The **skd** topology is relatively simple [56]. According to the TopCryst service of the Samara Topological Data Center [57], the **skd** net had previously been observed in molecular structures only, where molecules are linked together by hydrogen, Coulomb, or van der Waals bonds [58–60]. Therefore, kuliokite-(Y) is the first example of an inorganic crystal structure with the **skd** topology of interpolyhedral linkage. The ideal space group of the **skd** network is *Imma*, which is a supergroup of the space group *Im* determined herein for kuliokite-(Y). Note that in the **skd** net, there is only one symmetrical kind of vertex. The symmetry lowering from *Imma* to *Im* with splitting of a single Y node into two symmetrically independent Y sites is, at least in part, driven by HREE fractionation.

The backbone of the **skd** network is the dense double chain formed by Y_3 triangles that actually correspond to the two chains of the type shown in Figure 5d. The spatial relations between the double Y chains and the Al-Si chains are shown in Figure 7b.

3.3. Hydrogen Bonding

As was mentioned above, inspection of electron density difference Fourier maps allowed us to locate one H position only, namely one associated with the O6 site. The local environment of the H site is shown in Figure 8. There are no obvious strong hydrogen bonds donated by the OH6 group. There are two F^- anions located at 2.178 Å from the H atom; however, these $H \cdots F$ distances are too long for the hydrogen bonds formed by fluorine atoms [61]. The bond valence sums associated with the O5 and O6 sites are equal to 1.22 and 1.10 v.u., respectively, which agrees well with their assignment to hydroxyl groups.

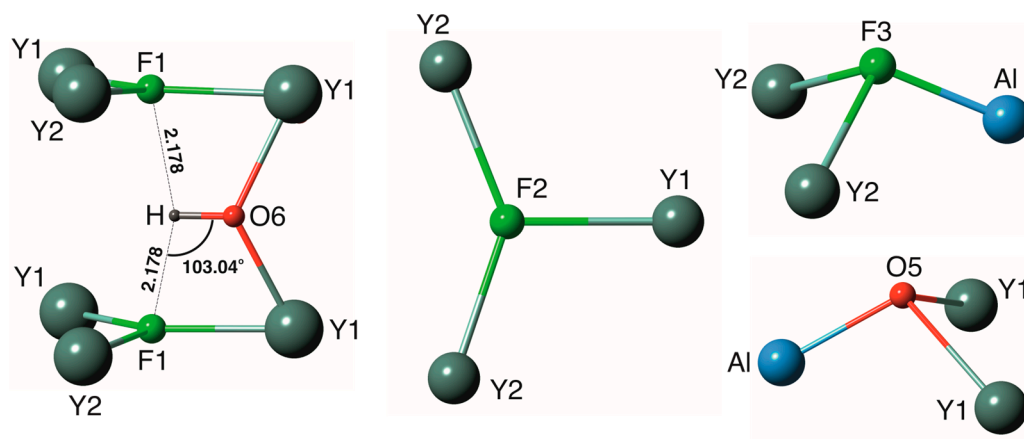


Figure 8. The local environment around the H site in the crystal structure of kuliokite-(Y), and the coordination of F and OH sites. Legend as in Figures 3 and 5.

4. Discussion

4.1. Rare Earth Fractionation

The crystal structure of kuliokite-(Y) represents a unique, in its transparency, example of REE fractionation governed by coordination mechanisms that involve lanthanide contraction. There are other minerals that display REE fractionation such as tveitite-(Y) [62], davidite-(La) [63], etc., and kuliokite-(Y) is another prominent example of such behavior.

4.2. Chemical Formula and Nomenclature Considerations

The original chemical formula of kuliokite-(Y) reported by Voloshin et al. [35] was given as $Y_4Al(SiO_4)_2(OH)_2F_5$. The ideal formula of our sample can be written as $Y_4Al[SiO_4]_2(OH)_{2.5}F_{4.5}$, which shows a higher OH content compared to the original samples. There are five X sites in kuliokite-(Y): F1, F2, F3, O5, and O6. The F1 and F2 sites form planar triangular groups (FY_3) with F atoms located within the planes defined by three Y atoms (Figure 8). It is rather unlikely that these sites may host hydroxyl groups. On the other hand, the O6 site is most likely the preferential site for hydroxyl and cannot be occupied by F^- anions. The F3 and O5 sites have very similar trigonal pyramidal coordination environments consisting of two Y and one Al atoms each (Figure 8). These sites can potentially be occupied by both F^- and $(OH)^-$ anions. If one of these sites is occupied by F and another by OH, the overall formula corresponds to the formula $Y_4Al(SiO_4)_2(OH)_2F_5$, which is the original formula of kuliokite-(Y) accepted by the International Mineralogical Association (IMA). If both F3 and O5 sites are occupied by fluorine, the formula should be written as $Y_4Al(SiO_4)_2(OH)F_6$, which corresponds to the potentially new mineral species, ‘fluorokuliokite-(Y)’. In contrast, the occupancy of both F3 and O5 sites by hydroxyl groups would lead to the formula $Y_4Al(SiO_4)_2(OH)_3F_4$ that could correspond to the species with the possible name ‘hydroxykuliokite-(Y)’. The sample studied in this work is therefore on the borderline between kuliokite-(Y) and ‘hydroxykuliokite-(Y)’. More analytical and structural research on material from different locations is needed in order to check whether ‘fluorokuliokite-(Y)’ and ‘hydroxykuliokite-(Y)’ exist in nature.

4.3. Optical Orientation

The revision of the symmetry of kuliokite-(Y) requires reconsideration of the optical orientation of the mineral. In the original work, the relations between crystallographic and optical axes were given as follows: $c_s = \gamma$, $\beta^\wedge b_s = 28^\circ$, $\alpha^\wedge a_s = 7^\circ$. Taking into account the changes in crystallographic axes described by Equation (1) above and the fact that $b_s^\wedge b_t = 30.7^\circ$ (rather close to the value of 28°), the correct optical orientation can be written

as $\alpha_t = \gamma$, $\beta = \mathbf{b}_t$, $\alpha^{\wedge} \mathbf{c}_t = 12.9^\circ$ (in obtuse β angle). Since $\alpha = 1.656(1)$, $\beta = 1.700(1)$, and $\gamma = 1.703(1)$ [35], kuliokite-(Y) has rather strong birefringence with the direction of maximal refraction corresponding to the direction of the aluminosilicate chains and the direction of minimal refraction oriented perpendicular to the planes of these chains. This kind of optical orientation is in agreement with the general principles of optical anisotropy observed for layered or pseudo-layered materials [64].

4.4. Comparison with Trimounsine

It is of interest that the crystal structure of kuliokite-(Y), when viewed in terms of its cationic network (Figure 7), is topologically related to the crystal structure of trimounsine-(Y), $\text{Y}_2\text{Ti}_2(\text{SiO}_4)\text{O}_5$ [65,66], a rare yttrium titanosilicate from the Trimouns talc deposit, Ariège, France. In trimounsine (Figure 9a), the basic structural unit is the $[\text{Ti}_2\text{O}_5(\text{SiO}_4)]$ chain consisting of the backbone chain of edge-sharing TiO_6 octahedra incrustated by single SiO_4 tetrahedra (Figure 9b,c). The titanosilicate chains are linked by Y^{3+} cations located in between the chains. The topology of linkage of YO_n polyhedra in trimounsine-(Y) is identical to that observed in kuliokite-(Y) and corresponds to the **skd** network topology (Figure 9d). The one-dimensional channels in the **skd** network are occupied by complex Ti-Si chain graphs shown in Figure 9c.

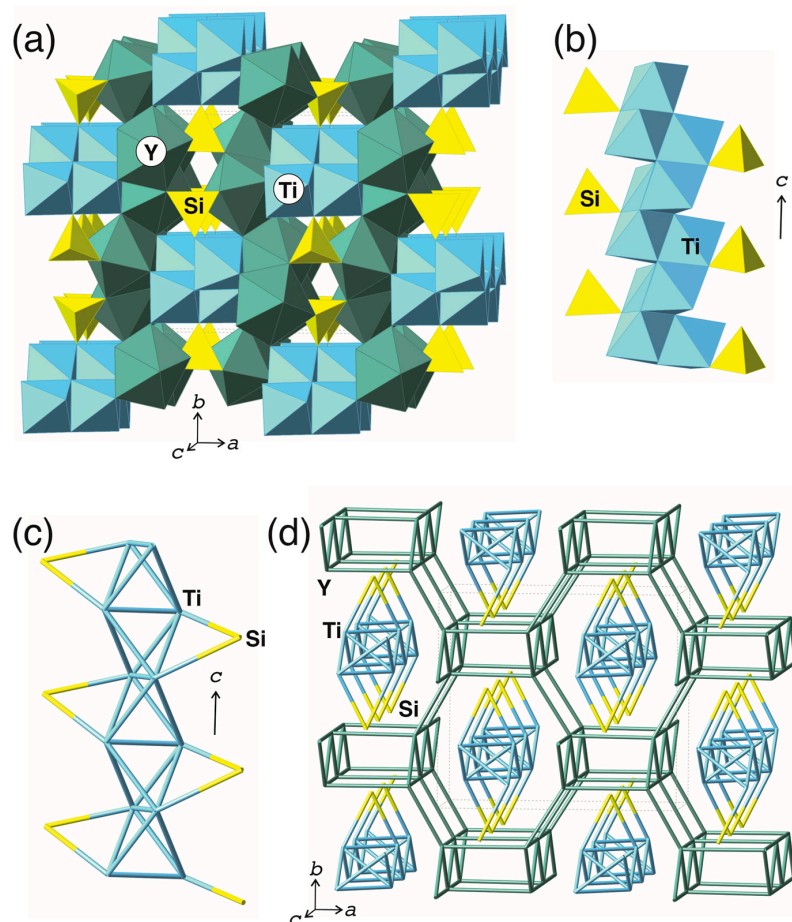


Figure 9. The crystal structure of trimounsine-(Y) in polyhedral representation (a) and its titanosilicate chain (b); the graph of the chain (c) and the crystal structure shown as the **skd**-type network with TiSi chain graphs in one-dimensional channels (d). Legend: Y polyhedral and Y nodes are shown in dark green; Ti polyhedral and Ti nodes are shown in light-blue; Si polyhedra and Si nodes are shown in yellow.

5. Conclusions

This crystal–chemical study of kuliokite-(Y) from the holotype locality allowed for the reconsideration of its symmetry as monoclinic with the non-centrosymmetric space group *Im*. The refinement of site occupancies indicated that the mineral represents a rare case of HREE fractionation among two cation sites driven by their coordination numbers and geometry. In agreement with the lanthanide contraction, HREEs are selectively incorporated into the site with a smaller coordination number and tighter coordination environment. The analysis of second-neighbor coordination of Y sites allowed us to identify the structural topology of kuliokite-(Y) as the only case of the **skd** network in inorganic compounds, previously known in molecular structures only. The variety of anionic content in the mineral allows us to identify the potential existence of two other mineral species that can tentatively be named as ‘fluorokuliokite-(Y)’ and ‘hydroxykuliokite-(Y)’.

Finally, it should be noted that, as to our knowledge, there are no known synthetic analogues of kuliokite-(Y). Taking into account the non-centrosymmetric nature of its crystal structure, it may be of interest to synthesize kuliokite and to investigate its physical properties [67]; doping with HREEs may play an essential role in its preparation.

Author Contributions: Conceptualization, S.V.K. and V.N.Y.; methodology, S.V.K., O.F.G., and Y.A.P.; validation, S.V.K.; formal analysis, S.V.K., O.F.G., and Y.A.P.; investigation, S.V.K., V.N.Y., O.F.G., and Y.A.P.; data curation, S.V.K.; writing—original draft preparation, S.V.K.; writing—review and editing, S.V.K. and V.N.Y.; visualization, S.V.K. and Y.A.P.; supervision, S.V.K.; project administration, S.V.K.; funding acquisition, S.V.K. All authors have read and agreed to the published version of the manuscript.

Funding: This research was funded in the framework of the state tasks FMEZ-2025-0070 (Nanomaterials Research Centre) and FMEZ-2024-0008 (Geological Institute) of the Kola Science Centre, Russian Academy of Sciences.

Data Availability Statement: The crystal structure data for kuliokite-(Y) are available as a CIF-file from the CCDC/FIZ Karlsruhe database under CSD # 2482967 at <https://www.ccdc.cam.ac.uk> (accessed on 8 October 2025).

Acknowledgments: The X-ray diffraction and chemical analytical studies were performed in the FRC KSC RAS Centre for Collective Use of Equipment.

Conflicts of Interest: The authors declare no conflicts of interest.

References

1. Kalashnikov, A.O.; Konopleva, N.G.; Pakhomovsky, Y.A.; Ivanyuk, G.Y. Rare Earth Deposits of the Murmansk Region, Russia—A Review. *Econ. Geol.* **2016**, *111*, 1529–1559. [CrossRef]
2. Goodenough, K.M.; Wall, F.; Merriman, D. The Rare Earth Elements: Demand, Global Resources, and Challenges for Resourcing Future Generations. *Nat. Resour. Res.* **2018**, *27*, 201–216. [CrossRef]
3. Foley, N.K.; Ayuso, R.A. Conventional Rare Earth Element Mineral Deposits—The Global Landscape. In *Rare Earth Metals and Minerals Industries: Status and Prospects*; Murty, Y.V., Alvin, M.A., Lifton, J.P., Eds.; Springer International Publishing: Cham, Switzerland, 2024; pp. 17–56.
4. Chen, P.; Ilton, E.S.; Wang, Z.; Rosso, K.M.; Zhang, X. Global Rare Earth Element Resources: A Concise Review. *Appl. Geochem.* **2024**, *175*, 106158. [CrossRef]
5. Shuai, Z.; Zhu, Y.; Gao, P.; Han, Y. Rare Earth Elements Resources and Beneficiation: A Review. *Miner. Eng.* **2024**, *218*, 109011. [CrossRef]
6. Campostrini, I.; Demartin, F.; Finello, G.; Vignola, P. Aluminotaipingite-(CeCa), (Ce₆Ca₃)Al(SiO₄)₃[SiO₃(OH)]₄F₃, a New Member of the Cerite-Supergroup Minerals. *Miner. Mag.* **2023**, *87*, 741–747. [CrossRef]
7. Holtstam, D.; Casey, P.; Bindi, L.; Förster, H.-J.; Karlsson, A.; Appelt, O. Fluorbritholite-(Nd), Ca₂Nd₃(SiO₄)₃F, a New and Key Mineral for Neodymium Sequestration in REE Skarns. *Miner. Mag.* **2023**, *87*, 731–737. [CrossRef]
8. Kampf, A.R.; Ma, C.; Marty, J. Chinleite-(Nd), NaNd(SO₄)₂(H₂O), The Nd analogue of chinleite-(Y) from the Markey Mine, Red Canyon, San Juan County, Utah, USA. *Can. J. Miner. Petrol.* **2023**, *61*, 411–418. [CrossRef]

9. Liu, P.; Gu, X.; Zhang, W.; Hu, H.; Chen, X.; Wang, X.; Song, W.; Yu, M.; Cook, N.J. Jingwenite-(Y) from the Yushui Cu Deposit, South China: The First Occurrence of a V-HREE-Bearing Silicate Mineral. *Am. Miner.* **2023**, *108*, 192–196. [\[CrossRef\]](#)
10. Lykova, I.; Rowe, R.; Poirier, G.; Friis, H.; Helwig, K. Mckelveyite Group Minerals Part 2: Alicewilsonite-(YCe), $\text{Na}_2\text{Sr}_2\text{YCe}(\text{CO}_3)_6 \cdot 3\text{H}_2\text{O}$, a New Species. *Eur. J. Miner.* **2023**, *35*, 143–155. [\[CrossRef\]](#)
11. Ondrejka, M.; Uher, P.; Ferenc, Š.; Majzlan, J.; Pollok, K.; Mikuš, T.; Milovská, S.; Molnárová, A.; Škoda, R.; Kopáček, R.; et al. Monazite-(Gd), a New Gd-Dominant Mineral of the Monazite Group from the Zimná Voda REE-U-Au Quartz Vein, Prakovce, Western Carpathians, Slovakia. *Miner. Mag.* **2023**, *87*, 568–574. [\[CrossRef\]](#)
12. Števkó, M.; Myšľan, P.; Biagioni, C.; Mauro, D.; Mikuš, T. Ferriandrosite-(Ce), a New Member of the Epidote Supergroup from Betliar, Slovakia. *Miner. Mag.* **2023**, *87*, 887–895. [\[CrossRef\]](#)
13. Wang, Y.; Gu, X.; Dong, G.; Hou, Z.; Nestola, F.; Yang, Z.; Fan, G.; Wang, Y.; Qu, K. Calcioancylite-(La), $(\text{La,Ca})_2(\text{CO}_3)_2(\text{OH,H}_2\text{O})_2$, a New Member of the Ancylite Group from Gejiu Nepheline Syenite, Yunnan Province, China. *Miner. Mag.* **2023**, *87*, 554–560. [\[CrossRef\]](#)
14. Wu, B.; Gu, X.-P.; Rao, C.; Wang, R.-C.; Xing, X.-Q.; Wan, J.-J.; Zhong, F.-J.; Bonnetti, C. Gysinite-(La), $\text{PbLa}(\text{CO}_3)_2(\text{OH})\text{H}_2\text{O}$, a New Rare Earth Mineral of the Ancylite Group from the Saima Alkaline Complex, Liaoning Province, China. *Miner. Mag.* **2023**, *87*, 143–150. [\[CrossRef\]](#)
15. Kasatkin, A.V.; Zubkova, N.V.; Škoda, R.; Pekov, I.V.; Agakhanov, A.A.; Gurzhiy, V.V.; Ksenofontov, D.A.; Belakovskiy, D.I.; Kuznetsov, A.M. The Mineralogy of the Historical Mochalin Log REE Deposit, South Urals, Russia. Part V. Zilbermintsite-(La), $(\text{CaLa}_5)(\text{Fe}^{3+}\text{Al}_3\text{Fe}^{2+})[\text{Si}_2\text{O}_7][\text{SiO}_4]_5\text{O}(\text{OH})_3$, a New Mineral with ET2 Type Structure and a Definition of the Radekškodaite Group. *Miner. Mag.* **2024**, *88*, 302–311. [\[CrossRef\]](#)
16. Liu, P.; Li, G.; Sun, N.; Yao, W.; Yu, H.; Tian, Y.; Yang, W.; Zhao, F.; Cook, N.J. Wenlanzhangite-(Y) from the Yushui Deposit, South China: A Potential Proxy for Tracing the Redox State of Ore Formation. *Am. Miner.* **2024**, *109*, 1738–1747. [\[CrossRef\]](#)
17. Lykova, I.; Rowe, R.; Poirier, G.; Friis, H.; Helwig, K. Mckelveyite Group Minerals—Part 3: Bainbridgeite-(YCe), $\text{Na}_2\text{Ba}_2\text{YCe}(\text{CO}_3)_6 \cdot 3\text{H}_2\text{O}$, a New Species from Mont Saint-Hilaire, Canada. *Eur. J. Miner.* **2024**, *36*, 183–194. [\[CrossRef\]](#)
18. Lykova, I.; Rowe, R.; Poirier, G.; Friis, H.; Helwig, K. Mckelveyite Group Minerals—Part 4: Alicewilsonite-(YLa), $\text{Na}_2\text{Sr}_2\text{YLa}(\text{CO}_3)_6 \cdot 3\text{H}_2\text{O}$, a New Lanthanum-Dominant Species from the Paratoo Mine, Australia. *Eur. J. Miner.* **2024**, *36*, 301–310. [\[CrossRef\]](#)
19. Ondrejka, M.; Bačík, P.; Majzlan, J.; Uher, P.; Ferenc, Š.; Mikuš, T.; Števkó, M.; Čaplovičová, M.; Milovská, S.; Molnárová, A.; et al. Xenotime-(Gd), a New Gd-Dominant Mineral of the Xenotime Group from the Zimná Voda REE-U-Au Quartz Vein, Prakovce, Western Carpathians, Slovakia. *Miner. Mag.* **2024**, *88*, 613–622. [\[CrossRef\]](#)
20. Pekov, I.V.; Zubkova, N.V.; Kasatkin, A.V.; Chukanov, N.V.; Koshlyakova, N.N.; Ksenofontov, D.A.; Škoda, R.; Britvin, S.N.; Kirillov, A.S.; Zaitsev, A.N.; et al. Hydroxylbastnäsité-(La), an “old New” Bastnäsité-Group Mineral. *Miner. Mag.* **2024**, *88*, 755–765. [\[CrossRef\]](#)
21. Pieczka, A.; Kristiansen, R.; Stachowicz, M.; Dumanska-Słowik, M.; Golebiowska, B.; Seęk, M.P.; Nejbert, K.; Kotowski, J.; Marciniak-Maliszewska, B.; Szuszkiewicz, A.; et al. Heflikite, Ideally $\text{Ca}_2(\text{Al}_2\text{Sc})(\text{Si}_2\text{O}_7)(\text{SiO}_4)\text{O}(\text{OH})$, the First Scandium Epidote-Supergroup Mineral from Jordanów Śląski, Lower Silesia, Poland and from Heftetjern, Tordal, Norway. *Miner. Mag.* **2024**, *88*, 228–243. [\[CrossRef\]](#)
22. She, H.; Liu, S.; Fan, H.; Gu, X.; Li, X.; Yang, K.; Wang, Q. Oboniobite and Scandio-fluoro-eckermannite, Two New Minerals in the Bayan Obo Deposit, Inner Mongolia. *Chin. J. Geol.* **2024**, *59*, 1466–1469. [\[CrossRef\]](#)
23. Yang, J.; Du, W. High-Pressure Minerals and New Lunar Mineral Changésite-(Y) in Chang’e-5 Regolith. *Matter Radiat. Extrem.* **2024**, *9*, 027401. [\[CrossRef\]](#)
24. Yao, W.; Liu, P.; Li, G.; Sun, N.; Yang, W.; Jiang, C.; Du, W.; Zhang, C.; Song, W.; Cook, N.J.; et al. Yuchuanite-(Y), $\text{Y}_2(\text{CO}_3)_3 \cdot \text{H}_2\text{O}$, a New Hydrous Yttrium Carbonate Mineral from the Yushui Cu Deposit, South China. *Am. Miner.* **2024**, *109*, 599–605. [\[CrossRef\]](#)
25. Zhu, Z.; Wang, D.; Yu, H.; Chen, Z.; Li, Y.; Li, J.; Ren, J. Discovery and Geological Significance of New Mineral Tantaloeschynite-(Ce). *Geol. Surv. China* **2024**, *11*, 1–10. [\[CrossRef\]](#)
26. Kampf, A.R.; Ma, C.; Marty, J. Chinleite-(Ce), $\text{NaCe}(\text{SO}_4)_2(\text{H}_2\text{O})$, a new mineral from the Blue Streak Mine, Montrose County, Colorado, USA. *Can. J. Miner. Petrol.* **2025**, *63*, 199–204. [\[CrossRef\]](#)
27. Malcherek, T.; Schlüter, J.; Husdal, T. Anorthoytttrialite-(Y), $\text{Y}_4(\text{SiO}_4)(\text{Si}_3\text{O}_{10})$, a Natural Representative of B-Type Rare Earth Disilicates. *Miner. Mag.* **2025**, *89*, 428–442. [\[CrossRef\]](#)
28. Plášil, J.; Steciuk, G.; Sejkora, J.; Kampf, A.R.; Uher, P.; Ondrejka, M.; Škoda, R.; Dolníček, Z.; Philippo, S.; Guennou, M.; et al. Extending the mineralogy of U^{6+} (I): Crystal structure of lepersonnite-(Gd) and a description of the new mineral lepersonnite-(Nd). *Miner. Mag.* **2025**, *89*, in press. [\[CrossRef\]](#)
29. Plášil, J.; Steciuk, G.; Škoda, R.; Philippo, S.; Guennou, M. Extending the mineralogy of U^{6+} (III): Pendevilleite-(Y), a new uranyl carbonate mineral from Kamoto-East Open-Cut, Democratic Republic of Congo. *Miner. Mag.* **2025**, *89*, in press. [\[CrossRef\]](#)
30. Buck, H.M.; Cooper, M.A.; Cerny, P.; Grice, J.D.; Hawthorne, F.C. Xenotime-(Yb), YbPO_4 , a New Mineral Species from the Shatford Lake Pegmatite Group, Southeastern Manitoba, Canada. *Can. Miner.* **1999**, *37*, 1303–1306.

31. Simmons, W.B.; Hanson, S.L.; Falster, A.U. samarskite-(Yb): A new species of the samarskite group from the Little Patsy pegmatite, Jefferson County, Colorado. *Can. Miner.* **2006**, *44*, 1119–1125. [\[CrossRef\]](#)
32. Voloshin, A.V.; Pakhomovsky, Y.A.; Men'shikov, Y.P.; Povarennykh, A.S.; Matvinenko, E.N.; Yakubovich, O.V. Hingganite-(Yb), a new mineral from amazonite pegmatites of the Kola Peninsula. *Dokl. AN. SSSR* **1983**, *270*, 1188–1192. (In Russian) [\[CrossRef\]](#)
33. Voloshin, A.V.; Pakhomovsky, Y.A.; Tyusheva, F.N. Keiviite $\text{Yb}_2\text{Si}_2\text{O}_7$ —A new ytterbium silicate from amazonitic pegmatites of the Kola Peninsula. *Mineral. Zhurnal* **1983**, *5*, 94–99. (In Russian)
34. Voloshin, A.V.; Pakhomovsky, Y.A. *Minerals and Evolution of Mineral Formation in Amazonitic Pegmatites of the Kola Peninsula*; Nauka: Leningrad, Russia, 1986. (In Russian)
35. Voloshin, A.V.; Pakhomovsky, Y.A.; Tyusheva, F.N.; Sokolova, E.V.; Egorov-Tismenko, Y.K. Kuliokite-(Y)—new yttrium-aluminum fluorosilicate from amazonitic pegmatites of the Kola Peninsula. *Mineral. Zhurnal* **1986**, *8*, 94–99. (In Russian)
36. Raade, G.; Saebo, P.C.; Austrheim, H.; Kristiansen, R. Kuliokite-(Y) and its alteration products kainosite-(Y) and kamphaugite-(Y) from granite pegmatite in Tordal, Norway. *Eur. J. Miner.* **1993**, *5*, 691–698. [\[CrossRef\]](#)
37. Husdal, T.A. The minerals of the pegmatites within the Tysfjord granite, Northern Norway. *Nor. Bergverksmus. Skr.* **2008**, *38*, 5–28.
38. Sokolova, E.V.; Egorov-Tismenko, Y.K.; Voloshin, A.V.; Pakhomovskii, Y.A. Crystal structure of the new Y-Al silicate kuliokite-(Y), $\text{Y}_4\text{Al}[\text{SiO}_4]_2(\text{OH})_2\text{F}_5$. *Sov. Phys. Crystallogr.* **1986**, *31*, 601–603.
39. Agilent Technologies. *CrysAlisPro*, Version 1.171.36.20; Agilent Technologies: Santa Clara, CA, USA, 2012.
40. Sheldrick, G.M. A short history of SHELX. *Acta Crystallogr.* **2008**, *A64*, 112–116. [\[CrossRef\]](#)
41. Spek, A.L. Single-Crystal Structure Validation with the Program It PLATON. *J. Appl. Crystallogr.* **2003**, *36*, 7–13. [\[CrossRef\]](#)
42. Flack, H.D. On enantiomorph-polarity estimation. *Acta Crystallogr. A* **1983**, *39*, 876–881. [\[CrossRef\]](#)
43. Gagné, O.C.; Hawthorne, F.C. Comprehensive Derivation of Bond-Valence Parameters for Ion Pairs Involving Oxygen. *Acta Crystallogr. B* **2015**, *71*, 562–578. [\[CrossRef\]](#)
44. Brese, N.E.; O'Keeffe, M. Bond-Valence Parameters for Solids. *Acta Crystallogr. B* **1991**, *47*, 192–197. [\[CrossRef\]](#)
45. Bandurkin, G.A.; Dzhurinskii, B.F.; Tananaev, I.V. *Peculiarities of Crystal Chemistry of Rare Earth Compounds*; Nauka: Moscow, Russia, 1984; p. 230. (In Russian)
46. Jordan, R.B. Lanthanide Contraction: What Is Normal? *Inorg. Chem.* **2023**, *62*, 3715–3721. [\[CrossRef\]](#)
47. Peters, J.A.; Djanashvili, K.; Geraldès, C.F.G.C.; Platas-Iglesias, C. The Chemical Consequences of the Gradual Decrease of the Ionic Radius along the Ln-Series. *Coord. Chem. Rev.* **2020**, *406*, 213146. [\[CrossRef\]](#)
48. Hawthorne, F.C.; Gagné, O.C. New Ion Radii for Oxides and Oxyalts, Fluorides, Chlorides and Nitrides. *Coord. Chem. Rev.* **2024**, *80*, 326–339. [\[CrossRef\]](#)
49. Schleid, T.; Müller-Bunz, H. Einkristalle von $\text{Y}_3\text{F}[\text{Si}_3\text{O}_{10}]$ Im Thalenit-Typ. *Z. Für Anorg. Und Allg. Chem.* **1998**, *624*, 1082–1084. [\[CrossRef\]](#)
50. Škoda, R.; Plášil, J.; Jonsson, E.; Čopjaková, R.; Langhof, J.; Galiová, M.V. Redefinition of Thalénite-(Y) and Discreditation of Fluorthalénite-(Y): A Re-Investigation of Type Material from the Österby Pegmatite, Dalarna, Sweden, and from Additional Localities. *Miner. Mag.* **2015**, *79*, 965–983. [\[CrossRef\]](#)
51. Shen, J.; Moore, P.B. Crystal structure of cappelenite, $\text{Ba}(\text{Y,RE})_6[\text{Si}_3\text{Be}_6\text{O}_{24}]\text{F}_2$: A silicoborate sheet structure. *Am. Miner.* **1984**, *69*, 190–195.
52. Krivovichev, S.V. Structure Description, Interpretation and Classification in Mineralogical Crystallography. *Crystallogr. Rev.* **2017**, *23*, 2–71. [\[CrossRef\]](#)
53. Krivovichev, S.V. Topology of Microporous Structures. *Rev. Miner. Geochem.* **2005**, *57*, 17–68. [\[CrossRef\]](#)
54. O'Keeffe, M.; Peskov, M.A.; Ramsden, S.J.; Yaghi, O.M. The Reticular Chemistry Structure Resource (RCSR) Database of, and Symbols for, Crystal Nets. *Acc. Chem. Res.* **2008**, *41*, 1782–1789. [\[CrossRef\]](#)
55. Reticular Chemistry Structure Resource. Available online: <http://rcsr.net/> (accessed on 8 October 2025).
56. Krivovichev, S.V. Which Nets Are the Most Common? Reticular Chemistry and Information Entropy. *CrystEngComm* **2024**, *26*, 1245–1251. [\[CrossRef\]](#)
57. Samara Topological Data Center. Available online: <https://topcryst.com/> (accessed on 8 October 2025).
58. Haase, M.G.; Günther, W.; Görls, H.; Anders, E. N-Heteroarylphosphonates, Part II. Synthesis and Reactions of 2- and 4-Phosphonatoquinolines and Related Compounds. *Synthesis* **1999**, *1999*, 2071–2081. [\[CrossRef\]](#)
59. Rehman, J.; Ejaz, Khan, I.U.; Harrison, W.T.A. N-(4-Aminophenyl)-4-Methylbenzene-Sulfonamide. *Acta Crystallogr. E* **2011**, *67*, o2709. [\[CrossRef\]](#) [\[PubMed\]](#)
60. Iwata, K.; Kojima, T.; Ikeda, Y. Solid Form Selection of Highly Solvating TAK-441 Exhibiting Solvate-Trapping Polymorphism. *Cryst. Growth Des.* **2014**, *14*, 3335–3342. [\[CrossRef\]](#)
61. Jeffrey, G.A. *An Introduction to Hydrogen Bonding*; Oxford University Press: New York, NY, USA; Oxford, UK, 1997; p. 303.
62. Yakubovich, O.V.; Massa, W.; Pekov, I.V.; Gavrilenko, P.G. Crystal Structure of Tveitite-(Y): Fractionation of Rare-Earth Elements between Positions and the Variety of Defects. *Crystallogr. Rep.* **2007**, *52*, 71–79. [\[CrossRef\]](#)
63. Gatehouse, B.M.; Grey, I.E.; Kelly, P.R. The Crystal Structure of Davidite. *Am. Miner.* **1979**, *64*, 1010–1017.

64. Pushcharovsky, D.Y. *Structures and Properties of Crystals*; GEOS: Moscow, Russia, 2022; p. 260.
65. Piret, P.; Deliens, M.; Pinet, M. La trimounsité-(Y), nouveau silicotitanate de terres rares de Trimouns, Ariège, France; $(\text{TR})_2\text{Ti}_2\text{SiO}_9$. *Eur. J. Miner.* **1990**, *2*, 725–729. [[CrossRef](#)]
66. Kolitsch, U. The crystal structure of trimounsité-(Y), $(\text{Y,REE})_2\text{Ti}_2\text{SiO}_9$: An unusual TiO_6 -based titanate chain. *Eur. J. Miner.* **2001**, *13*, 761–768. [[CrossRef](#)]
67. Bindi, L.; Nespolo, M.; Krivovichev, S.V.; Chapuis, G.; Biagioni, C. Producing Highly Complicated Materials. Nature Does It Better. *Rep. Progr. Phys.* **2020**, *83*, 106501. [[CrossRef](#)] [[PubMed](#)]

Disclaimer/Publisher’s Note: The statements, opinions and data contained in all publications are solely those of the individual author(s) and contributor(s) and not of MDPI and/or the editor(s). MDPI and/or the editor(s) disclaim responsibility for any injury to people or property resulting from any ideas, methods, instructions or products referred to in the content.